Dentomaxillofacial Radiology (2014) 43, 20130273

http://dmfr.birjournals.org

RESEARCH

Regional 3D superimposition to assess temporomandibular joint condylar morphology

J Schilling*[,1], L C R Gomes[2], E Benavides[1], T Nguyen[3], B Paniagua[4], M Styner[4], V Boen[5], J R Gonçalves[2] and L H S Cevidanes[5]

[1]Department of Periodontics and Oral Medicine, School of Dentistry, University of Michigan, Ann Arbor, MI, USA; [2]Department of Orthodontics and Pediatric Dentistry, Araraquara Dental School, UNESP Univ Estadual Paulista, Araraquara, Sao Paulo, Brazil; [3]Department of Orthodontics, School of Dentistry, University of North Carolina, Chapel Hill, NC, USA; [4]Department of Psychiatry, School of Medicine, University of North Carolina, Chapel Hill, NC, USA; [5]Department of Orthodontics and Pediatric Dentistry, University of Michigan, Ann Arbor, MI, USA

Objectives: To investigate the reliability of regional three-dimensional registration and superimposition methods for assessment of temporomandibular joint condylar morphology across subjects and longitudinally.

Methods: The sample consisted of cone beam CT scans of 36 patients. The across-subject comparisons included 12 controls, mean age 41.3 ± 12.0 years, and 12 patients with temporomandibular joint osteoarthritis, mean age 41.3 ± 14.7 years. The individual longitudinal assessments included 12 patients with temporomandibular joint osteoarthritis, mean age 37.8 ± 16.7 years, followed up at pre-operative jaw surgery, immediately after and one-year post-operative. Surface models of all condyles were constructed from the cone beam CT scans. Two previously calibrated observers independently performed all registration methods. A landmark-based approach was used for the registration of across-subject condylar models, and temporomandibular joint osteoarthritis *vs* control group differences were computed with shape analysis. A voxel-based approach was used for registration of longitudinal scans calculated x, y, z degrees of freedom for translation and rotation. Two-way random intraclass correlation coefficients tested the interobserver reliability.

Results: Statistically significant differences between the control group and the osteoarthritis group were consistently located on the lateral and medial poles for both observers. The interobserver differences were ≤0.2 mm. For individual longitudinal comparisons, the mean interobserver differences were ≤0.6 mm in translation errors and 1.2° in rotation errors, with excellent reliability (intraclass correlation coefficient >0.75).

Conclusions: Condylar registration for across-subjects and longitudinal assessments is reliable and can be used to quantify subtle bony differences in the three-dimensional condylar morphology.

Dentomaxillofacial Radiology (2014) **43,** 20130273. doi: 10.1259/dmfr.20130273

Cite this article as: Schilling J, Gomes LCR, Benavides E, Nguyen T, Paniagua B, Styner M, et al. Regional 3D superimposition to assess temporomandibular joint condylar morphology. *Dentomaxillofac Radiol* 2014; **43:** 20130273.

Keywords: temporomandibular joint; reliability; measurements; registration; condyle; morphology

Introduction

The temporomandibular joint (TMJ) is a complex joint that is submitted to high loading activity, often owing to parafunctional oral habits or to alterations of the stomatognathic system. The health of a TMJ depends on the capacity of its joint components to adapt to normal

*Correspondence to: Dr Juan Schilling, Department of Periodontics and Oral Medicine, School of Dentistry, University of Michigan, 1011 North University Avenue, Ann Arbor, MI 734-936-6282, USA. E-mail: juan.schilling@gmail.com
This study has been funded by the American Association of Orthodontists Foundation.
Received 28 July 2013; revised 3 October 2013; accepted 22 October 2013

or abnormal function. TMJ pathologies that result in alterations to the size, form, spatial and functional relationships of the joint components can lead to progressive changes and compensations that may ultimately affect the jaw and tooth positions and occlusion.

Recent studies have shown that TMJ osteoarthritis (OA) is a local inflammatory condition which occurs when the dynamic equilibrium between the breakdown and repair of the joint tissue is compromised.[1–3] The spectrum of the clinical and pathological presentation of TMJ OA ranges from structural and functional failure of the joint with disc displacement and degeneration to subchondral bone alterations (erosions), bone overgrowth (osteophytes), loss of articular fibrocartilage and synovitis. Altered bone morphology[4,5] and associated mechanical properties may distort joint mechanics, leading to joint degeneration such as that shown in Figure 1. The exact role of the bone under the articular cartilage in the aetiology of arthritis is unclear. Much of our understanding of arthritic bone changes comes from animal models or cadaveric specimens as opposed to assessments of patients with arthritis. Quantification of three-dimensional (3D) bony changes is critical to compare the ability of different treatment modalities to arrest progression of bone destruction (*i.e.* methotrexate, biological agents such as anti-tumour necrosis factor α[6,7] or surgical interventions).[8,9]

The Research Diagnostic Criteria for Temporomandibular Disorder validation project[10–12] concluded that clinical criteria alone, without the use of imaging, are inadequate for valid diagnosis of TMJ arthritis. The application of cone beam CT (CBCT) to craniofacial imaging provides a clear visualization of the hard tissues of TMJ and markedly reduces radiation and cost compared with medical CT.[13–23] The Osteoarthritis Initiative, a National Institutes of Health-sponsored consortium, focused on identifying imaging biomarkers of development and progression of knee OA using MRI.[24] Although ultrasound and MRI are effective in monitoring synovitis,[25–27] MRI and panoramic radiography have poor to marginal sensitivity in detecting arthritic bony changes in TMJ.[11] CBCT has recently replaced other imaging modalities and become the modality of choice to study TMJ arthritic bony changes because it provides high-quality images for quantification of bone changes, such as erosions, osteophytes, flattening, sclerosis and abnormal condylar shape.[22,23,28] However, the standardization of cross sections in the assessment of multiplanar images is challenging in longitudinal and across-subject studies. The use of 3D surface models and quantitative morphological assessments now offers the possibility of additional diagnostic information that is difficult to achieve by assessing the multiplanar images. This study proposes methods for the registration of 3D condylar morphology as essential procedures for the measurement of subtle bony differences in condylar morphology. Specifically, the aims of this study were to test the reliability of regional superimposition techniques for populational across-subject comparisons and for the assessment of bony changes on serial CBCT scans in longitudinal studies.

Materials and methods

Sample

The sample consisted of CBCT scans from 36 patients acquired for a parent study. All the scans were taken with an i-Cat® CBCT (120 kV, 18.66 mA; Imaging Sciences International, Hatfield, PA). The secondary analysis of deidentified CBCT data in this study was approved by the university institutional review board. These scans included two independent samples for across-subject and longitudinal experiments. After clinical examination and diagnosis of TMJ OA or health, a 20 s cone beam CT scan with 0.3 mm original resolution was obtained for all participants, using a large field of view to include both TMJs.

The sample to test the reproducibility of across-subject and group comparisons included surface models of 48 right and left condyles constructed from CBCT scans of 12 healthy control subjects, with a mean age of 41.3 ± 12.0 years, and 12 patients with a clinical diagnosis of OA, with a mean age of 41.3 ± 14.7 years.

The sample to test the reproducibility of individual longitudinal assessments included surface models of 24 condyles constructed from CBCT scans acquired at 3 time points for 12 patients with a clinical diagnosis of TMJ OA[10] (mean age, 37.8 ± 16.7 years): before surgery (Time 1), immediately after jaw surgery (Time 2) and 1 year after jaw surgery (Time 3). All patients in this study sample presented marked skeletal discrepancies between the maxilla and the mandible. Selection of the appropriate radiographical imaging techniques was approved by the institutional review board based on the principle that each radiation exposure was justified clinically and that all appropriate measures to minimize patient radiation exposure while optimizing maximal diagnostic benefit were taken.

Image analysis methods

To standardize voxel size, all scans were resliced to a voxel size of 0.5 mm^3, to decrease the computational power and time required to compute the automated registration, using 3D Slicer v. 4.2.2 (open-source software, http://www.slicer.org).[29] The flow chart in Figure 2 describes an overview of the image analysis procedures for the regional 3D superimposition of mandibular condyles.

Construction of surface models (segmentation): The process of construction of surface models to perform the regional superimposition is called segmentation and was performed using the ITK-SNAP software v. 2.4 (open-source software, www.itksnap.org).[30–33] Segmentation of the right and left mandibular condyles consisted of outlining the cortical boundaries of the condylar region using semi-automatic and manual discrimination procedures that allowed manual editing, checking slice by slice in all three planes of space (sagittal, coronal and axial). The output of the ITK-SNAP segmentation was a 3D surface mesh reconstruction model. In this study, the surface mesh was saved as a binary *.stl (stereolithography) file for the across-subject

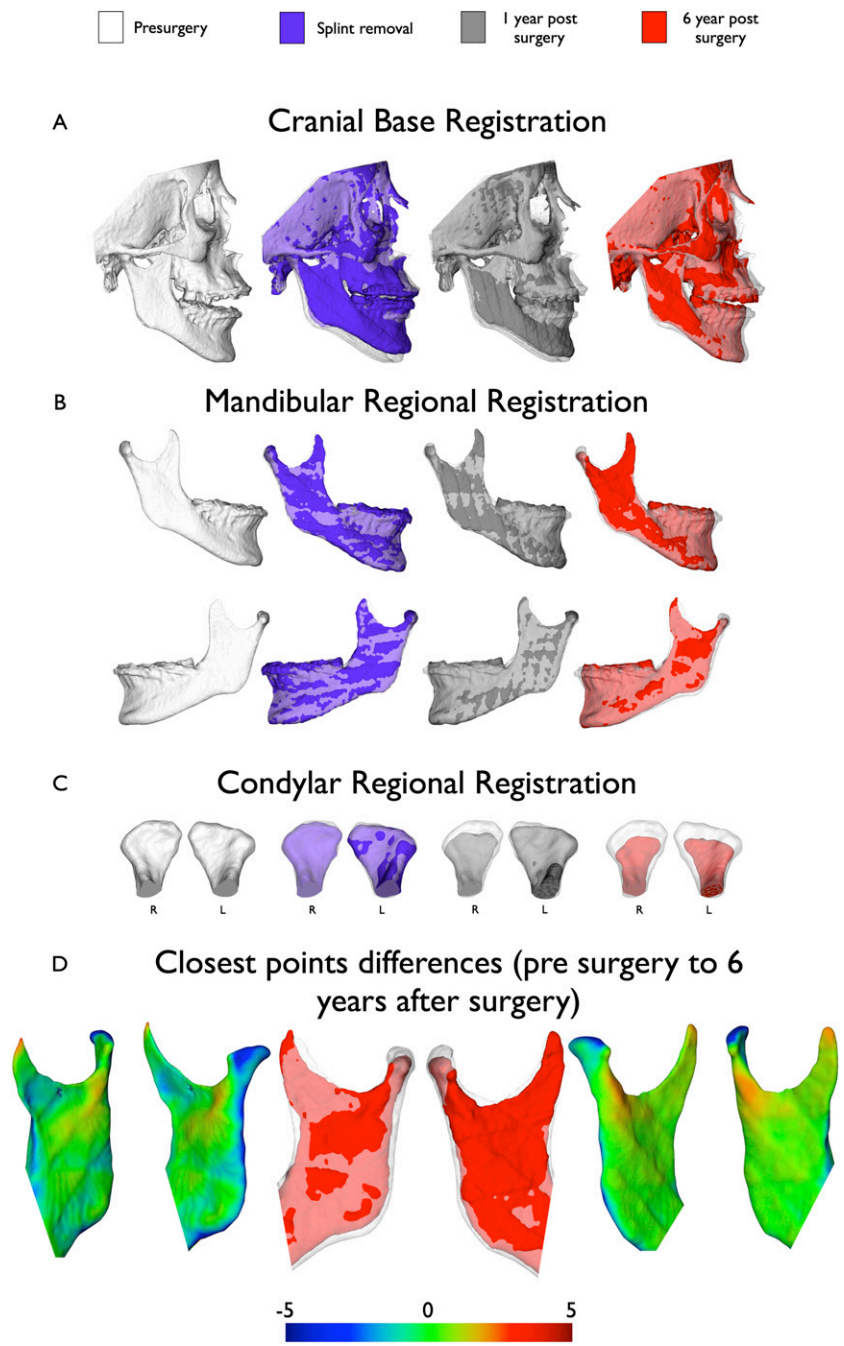

Figure 1 Clinical relevance of condylar and ramus adaptive bone remodeling changes over 6 years of follow-up for a patient who was treated with maxillary impaction for correction of open bite, as seen in the pre-surgery model (white) voxel-based automated registration is used using different anatomical structures of interest for reference to assess in detail the bone remodeling over time. (a) Cranial base superimposition with the pre-surgery model shown as a white semi-transparent overlay with the surface model at splint removal (blue), 1 year post-surgery (grey) and 6 years post-surgery (red). (b) Mandibular overall changes in a mandibular regional superimposition. Note the condylar changes and overall ramus adaptive changes that had began as shown in the overlay between pre surgery and 1 year post surgery and progressed a further 6 years post surgery. (c) Condylar regional superimposition showing the progression of condylar resorptive changes in more detail. (d) Close-up views of the left and right ramus changes between pre surgery and 6 years post surgery in a mandibular regional superimposition. The colour maps show about 5 mm of condylar changes and in some regions in the ramus surface. Colour visible in online version only

comparisons or as a *.gipl (guys image processing lab) volume file for the longitudinal assessments.

Registration: Two observers, one oral and maxillofacial radiologist (JS) and one orthodontist (LRG) collaborated to perform the regional registration across subjects and of serial CBCT images using sets of images not included in this study. After calibration, each observer analysed the CBCT scans independently, performing all registration procedures described below.

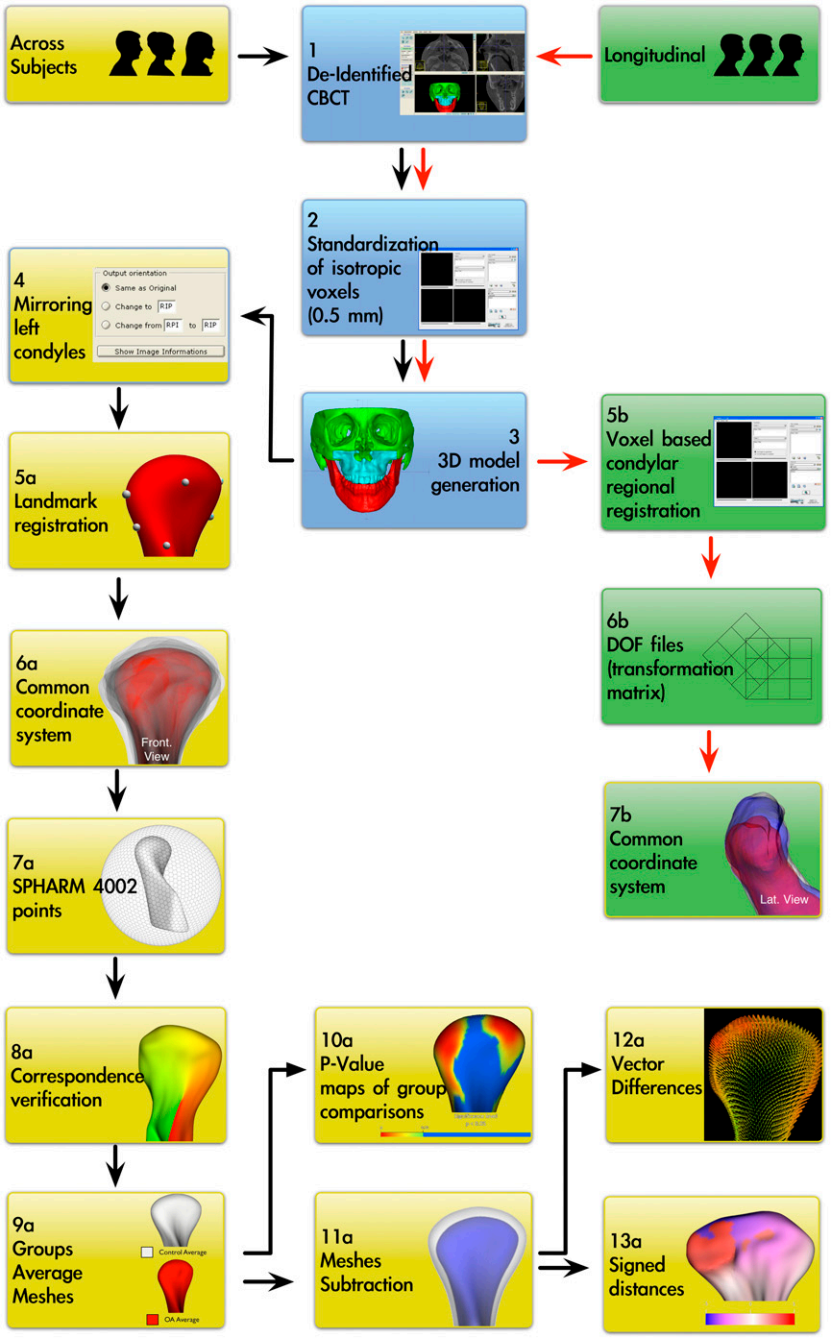

Figure 2 Study methodology flowchart. 3D, three dimensional; CBCT, cone beam CT; DOF, degrees of freedom; Lat, lateral; OA, osteoarthritis; SPHARM, SPHARM-PDM software v. 1.12 output of 4002 surface points

Across-subject and group comparisons

Mirroring: Left condyles were mirrored to form right condyles using Imconverter software v. 1.2 (open-source http://www.ia.unc.edu/dev/download/imconvert/index.htm)[34] to assess the morphology of all condyles in the same co-ordinate system.

Standardization of co-ordinate system—landmark-based registration: Owing to great individual morphological variability across subjects, voxel-based approaches fail and a landmark-based approach to consistently approximate all condyles in the same co-ordinate system was tested in this study. The .stl surface mesh files for each condyle were opened in VAM® v. 3.7.6 (Canfield Scientific Inc., Fairfield, NJ),[35] and 25 landmarks were placed on each condylar surface model: 4 points evenly spaced along the superior surface of the sigmoid notch, 4 on the medial and lateral portions of the ramus adjacent

to the sigmoid notch, 3 along the posterior neck of the condyle, 3 on the medial portion and 3 on the lateral portion of the condylar neck and on the medial, lateral, anterior, and posterior extremes of the condylar head (Figure 3A). Using a landmark-to-landmark best-fit alignment, each condyle was approximated to a chosen reference condyle; the reference condyle was one of the reconstructed condyles that presented preserved and clearly defined anatomical surfaces (lateral and medial poles, a well-defined sigmoid notch and the posterior border of the mandibular ramus), to establish a common co-ordinate system where all the individual condyles are approximated within the three-dimensional space (Figure 3B). The condyles were then simultaneously cropped to consistently define the region of interest using a line perpendicular to the long axis of the mandibular condyle, passing through the deepest point of the sigmoid notch.

Computation of corresponding points between all condyles: SPHARM-PDM software v. 1.12 (open-source, http://www.nitrc.org/projects/spharm-pdm)[32,33,36,37] was then used to compute the correspondence across 4002 surface points among all right and mirrored left condyles. These 4002 surface points and the location of their respective *XYZ* coordinates were optimized for each corresponding condyle mesh.

Quality control of the correspondence across all data sets: SPHARM-PDM output of 4002 correspondent point-based condylar models determined co-ordinate poles on each model that allow these point-based models to be displayed as colour-coded maps. Maps for each condyle model could be visually compared with each other to confirm that the parameterization was consistent across all condyles (Figure 4).

Creation of the average mesh: The core of the ability to compute the group average and group variability is the establishment of correspondence for each point in the surface models. This allows the association of any location on the condyle of subject A with the corresponding location on the condyle of subject B. Considerable intersubject variability is also accounted for in the model that captures the average condylar morphology and variability around that average morphology. A Linux MeshMath script (open-source software, http://www.nitrc.org/projects/spharm-pdm)[37] was used to create average meshes based on all condyles in the OA group and all condyles in the control group. The 4002 original surface point correspondences were propagated through all stages of deformations and were used for surface mesh averaging. The affine transformations were then applied to the points individually. In geometry, an affine transformation is a transformation which preserves ratios of distances between points lying on a surface model, where parallel lines will remain parallel to each other after an affine transformation. Grouping all the mean points provided the linear and nonlinear deformation fields that resulted in the average condyle shape for each group.

Calculation of absolute and vector differences and signed distances: The MeshMath script was then used to calculate 3D point-wise subtractions between the groups' average morphology. The computed 4002 vector differences were displayed on the condyle surface, 1 for each point on the surface mesh, scaled according to the magnitude of difference and pointing in the direction of change. The patterns of variation across TMJ OA and control samples were determined through calculation of signed distances, where the areas of bone resorption were displayed as negative values (blue), no differences (0 mm surface distances, white) or bone proliferation as positive (red).

Control of the quality of the signed distances: Semi-transparent overlays between the average models in 3D Slicer software were used to visually compare the signed distance patterns for both observers. The signed distance maps were used to qualitatively assess whether the areas of differences were consistent and quantitatively compare the measured 3D signed distances between the observers.

Longitudinal assessments

Voxel-based registration: The first step in the voxel-based registration of longitudinal scans was to manually approximate the CBCT scans taken at different time points using the 3D Slicer software to facilitate the automated voxel-based registration. The registration

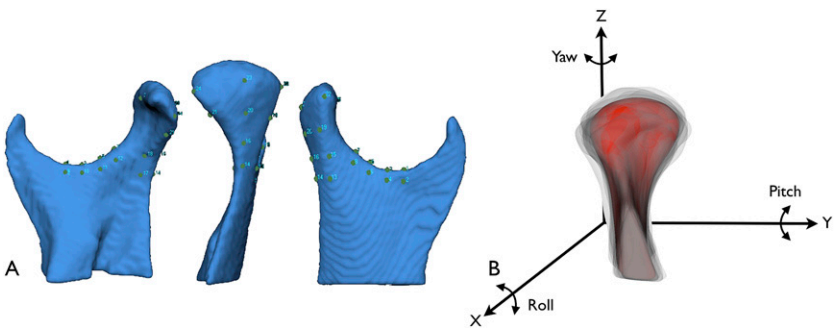

Figure 3 Landmark-based registration used to approximate condyles from all subjects in the group comparisons. (a) 25 points in the ramus and condyle surfaces used for landmark-based registration, (b) reference condylar model (red) with the overlay of multiple condyles approximated in the same co-ordinate system. Colour visible in online version only

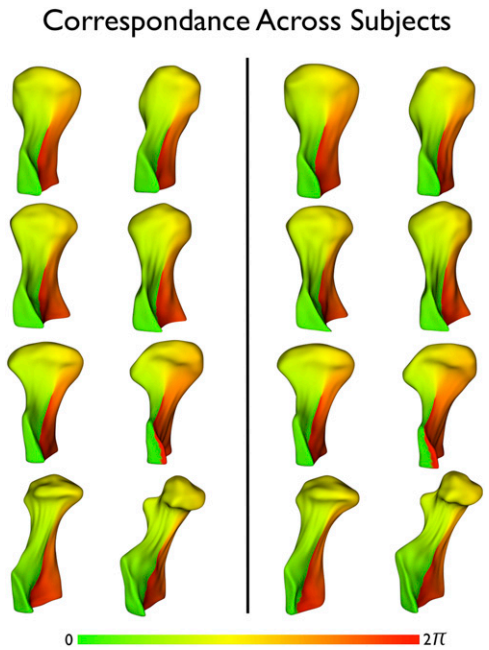

Figure 4 Quality control of the correspondence across 4002 points in the condylar surface models and between observers using parametric colour maps. These colour maps display one of the two spherical parameters, Phi, which is equivalent to geographical longitude. Eight condyles in the Observer 1 evaluation are shown in the left columns and the same condyles in Observer 2 evaluation are shown in the right columns. Note the consistency of the colour maps across all condyles and between observers. Colour visible in online version only

was then performed using the 3D Slicer craniomaxillofacial registration module (CMFreg, open source software, http://www.nitrc.org/plugins/mwiki/index.php/cmfreg:MainPage).[38] The software compares the intensity greyscale for each voxel of the images at pre surgery, splint removal and 1 year post surgery, to avoid observer-dependent reliance on subjectively defined anatomical landmarks. This procedure extracts the mandibular condyles as the region of interest, generating CBCT images that contain only the right or left condyle. All follow-up, scans were registered to the pre-surgery CBCT scan as a reference. The automatic registration outputs three files for split-removal and 1 year post-treatment time points: a registered CBCT image, a registered condyle surface model and a text file with the transformation matrix used to change the position of these images with six degrees of freedom (DOF) when registered to the pre-surgery image. The DOF text file contains information of the translation on the *X*t, *Y*t and *Z*t axes, respectively, of left–right, anteroposterior and inferosuperior displacements and on the rotation of the sagittal axis up and down (*X*r, pitch), the coronal axis mediolaterally (*Y*r, roll) and the axial axis mediolaterally (*Z*r, yaw).

Statistical analysis

Statistical shape analyses were carried out to test cross-patient group differences as measured by both observers. A multivariate analysis of covariance (http://www.nitrc.org/projects/shape_mancova)[39] is a statistical shape analysis method that allows for a localized analysis of shape.[40] Multivariate analysis of covariance was used in this study to estimate and compare average group morphology model of control and of TMJ OA patients, the average TMJ OA for Observer 1 *vs* Observer 2 and the average control for Observer 1 *vs* Observer 2. The *p*-value maps ($p < 0.05$) for testing group differences were calculated using Hotelling's T-squared metric based on covariance matrices.

The registration procedures for longitudinal assessments are automatic and avoid observer-dependent errors such as training and fatigue. For this reason, systematic error was not included in the statistical model. The intraclass correlation coefficient (ICC) was computed using SPSS® v. 20 (SPSS Inc., Chicago, IL) statistical analysis suite. A two-way random effect ICC model and its 95% confidence interval (CI) were used to test the interobserver variability of DOF values of the translation and rotation axes for all subjects.

Results

The semi-transparent overlays, vector and signed distance differences in Figure 5 graphically display the location

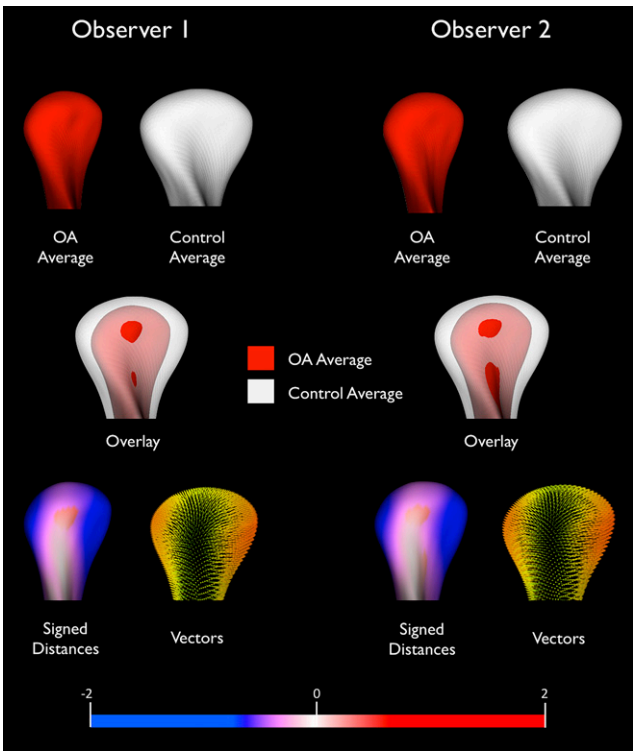

Figure 5 Group comparison results for both observers. The top row shows the group average models [temporomandibular joint osteoarthritis (TMJ OA) group in red and control group in white]. The middle row shows semi-transparent overlays for group comparisons. Note the similar patterns for both observers findings with slight difference in the anterior portion of condylar neck. The bottom row shows the colour maps of the quantitative subtractions both as signed colour-coded maps (where blue indicates areas of bone loss in the TMJ OA group and red indicates areas of bone proliferation). Colour visible in online version only

and magnitude of the group average comparisons showing similar patterns for both observers.

Statistically significant differences between the control group and the OA group were consistently located on the lateral and medial poles for both observers (Figure 6), with small interobserver differences in the extension of the significant areas shown in the *p*-value colour map. The interobserver differences were ≤0.18 mm (Table 1). The multivariate analysis of covariance group comparisons of the average TMJ OA morphology for Observer 1 *vs* Observer 2 and the average control morphology for Observer 1 *vs* Observer 2 were not significant.

Figure 7 illustrates the results of the longitudinal registration for one of the patients treated with bi-maxillary advancement surgery, where small changes in the superior condylar surface were found between pre-surgery and splint removal (2 months interval between the scans), and the progression of bone destruction with marked resorption of the superior articulating surface of the condyle at 1 year post surgery. Table 2 shows the descriptive statistics of the interobserver differences for the six DOFs in the automatic voxel-base registration of the serial CBCT condylar images. No right or left differences were observed and, for this reason, their absolute values were averaged. The direction of the registration of six DOFs (displacements on anteroposterior, inferosuperior, left–right translational axes or rotation of the sagittal axis up–down, coronal and axial axes yaw mediolaterally) showed concordance for between observers in all cases and the amount measured presented only small variability. The mean interobserver differences were smaller than 0.6 mm in translation errors and 1.2° in rotation errors, with excellent reliability (ICC > 0.75). For the pre-surgery to splint removal superimposition, the *Z* axis of translation (left–right) presented a mean interobserver error of 0.6 ± 0.8 mm (ICC = 0.81, lower limit of the 95% CI = 0.55). For the splint removal to 1 year post surgery superimposition, the *Y* axis of translation (anteroposterior) presented a mean interobserver error of 0.4 mm ± 0.5 mm (ICC = 0.76, lower limit of the 95% CI = 0.45) and the *Z* axis of rotation (axial, yaw) presented a mean interobserver error of 0.7 ± 0.8° (ICC = 0.8, lower limit of the 95% CI = 0.53).

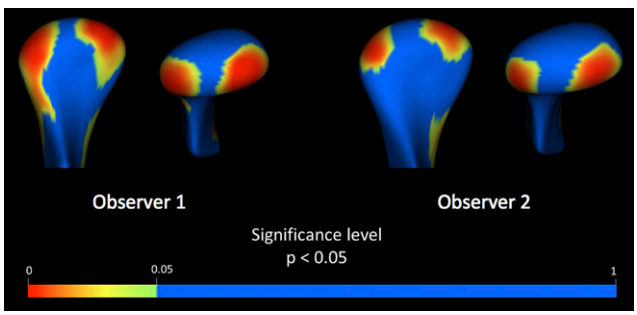

Figure 6 The *p*-value colour maps of areas of statistically significant differences between the control group and the temporomandibular joint osteoarthritis (TMJ OA) group. Similar statistical significance was found by both observers, with some variability in the extent of areas of the statistically significant differences between TMJ OA and control groups. Colour visible in online version only

Table 1 Surface distances (in millimetres) of the subtraction of average control and temporomandibular joint osteoarthritis condylar morphology

Group comparisons	*Observer 1*	*Observer 2*	*Interobserver differences*
Bone loss at the superior surface of the medial and lateral poles	−2.8	−2.7	−0.1
Bone proliferation at the anterior surface	13	1.1	0.2

Discussion

This study tested the reliability of the novel methods for registration of 3D condylar morphology, across subjects and longitudinally, as described above. The registration, superimposition and quantitative assessments across subjects have diagnostic applications, whereas the registration

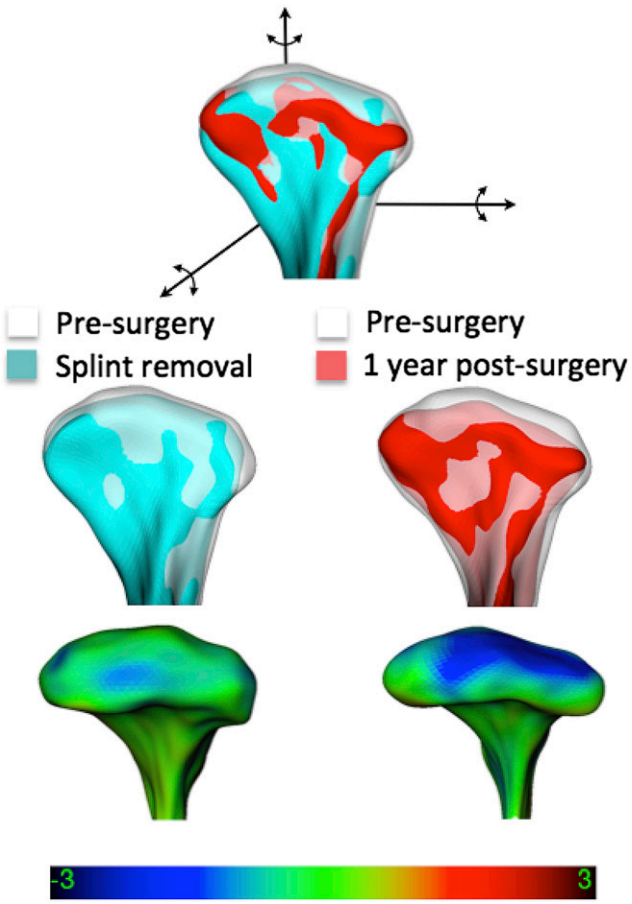

Figure 7 Longitudinal registration of the left condyle of a patient treated with bi-maxillary advancement. The top row shows the three time points registered and overlaid in the same co-ordinate system. The middle row shows the superimposition of pre-surgery (white) to splint removal (cyan) and pre-surgery to 1 year post-surgery (red). The bottom rows show closest point surface distances colour-coded maps showing slight condylar resorption in the 2 months between the pre-surgery and splint– removal scans and more the progression of the bone resorption at 1 year post-surgery. Colour visible in online version only

Table 2 Descriptive statistics and intraclass correlation coefficients (ICCs) for the interobserver variability in the six degrees of freedom computed for registration of CBCT scans at three time points

		Interobserver differences			*95% Confidence interval of the ICC*	
Registration	*Degrees of freedom*	*Mean*	*Standard deviation*	*ICC*	*Lower*	*Upper*
Pre-surgery to splint removal	Translation (mm)					
	*X*t	0.2	0.2	0.98	0.94	0.99
	*Y*t	0.4	0.4	0.92	0.81	0.97
	*Z*t	0.6	0.8	0.81	0.55	0.92
	Rotation (degrees)					
	*X*r	1.2	1.0	0.94	0.85	0.97
	*Y*r	0.7	0.8	0.92	0.82	0.97
	*Z*r	0.5	0.5	0.95	0.88	0.98
Pre-surgery to 1 year post surgery	Translation (mm)					
	*X*t	0.2	0.2	0.99	0.97	0.99
	*Y*t	0.4	0.5	0.76	0.45	0.90
	*Z*t	0.5	0.5	0.92	0.82	0.97
	Rotation (degrees)					
	*X*r	0.9	1.0	0.95	0.89	0.98
	*Y*r	0.5	0.7	0.94	0.86	0.98
	*Z*r	0.7	0.8	0.80	0.53	0.92

*X*r, *Y*r and *Z*r are the pitch, roll and yaw, respectively.

of longitudinal scans can be applied for the assessment of growth, progression of disease, treatment outcome and stability after treatment.[41]

The methods used in this study included open source image analysis software. Commercial software packages, such as Geomagic (Geomagic Inc., Morrisville, NC)[42,43] InVivo (Anatomage, San Jose, CA),[44,45] Maxilim (Medicim, Mechelen, Belgium),[46,47] OnDemand 3D™ (CyberMed, Seoul, Republic of Korea)[48] and Amira® (Visualization Sciences Group, Burlington, MA)[49] produce adequate surface reconstructions and/or offer landmark, surface and/or voxel-based registration methods, but they are not open source, cannot be modified, do not interact well with each other, do not provide flexibility for customization and, moreover, do not address the 3D correspondence problem across patients with different facial morphology or from pre- and post-surgery scans of the same patient. Software development in 3D image analysis is structurally different than it was a decade ago owing to the maturation of open source libraries like the Visualization ToolKit (VTK),[50] the National Library of Medicine Insight Segmentation and Registration Toolkit (ITK)[51,52] and of open source development tools, such as SVN and CMake.[53] More recently, whole software frameworks for medical image analysis have become available as open source, such as OsiriX (Pixmeo, Bernex, Switzerland)[54] for radiological applications and 3D Slicer[29] for general medical image processing and interventional guidance. Owing to its open licensing, 3D Slicer is increasingly being adopted as an interactive medical imaging platform. 3D Slicer v. 4 provides powerful tools for multimodal imaging, volume rendering, registration and visualization. All these open access or open source developments have contributed significantly to the field of medical image analysis and now have potential applications in dentistry as well.

As part of the methodology used in this study, the regional condylar registration required a number of different procedures for across-subject/group experiments compared with the longitudinal experiments. The differences in the methods of the two experiments are three-fold. First, the group comparisons in this study used mirroring techniques where left condyles were mirrored to form right condyles and allowed morphological comparisons. Right and left condylar changes were assessed separately in longitudinal studies, but right and left differences in interobserver errors were not observed, and for this reason, their absolute values were averaged.

Second, owing to great individual morphological variability across subjects, rigid voxel-based approaches (which compute differences in rotation, translation with or without scaling) fail to register anatomical structures from different subjects in populational or group average studies. Other voxel-based registration approaches, that are fluid or semi-fluid, deform the surface models,[55] and the deformation or morphing would hamper adequate evaluation of individual morphology. For these reasons, the registration across subjects in this study used an initial landmark-based approach to approximate all condyles in the same co-ordinate system as shown in Figure 3. Although this initial procedure was observer-dependent for manual identification of landmark locations, it only aimed to approximate all condyles and allow the automatic computation of 4002 correspondent surface points for all condyles in a consistent way, as highlighted by the very similar findings for both observers independently shown in Table 1 and Figures 4–6. In the present study, the intersubject variability was also accounted for in the model that captures the average condylar morphology and variability around that average morphology.

Third, the sequence of procedures for longitudinal registration is simpler than across-subject registration (flowchart in Figure 2). The voxel-based approach for longitudinal registration outputs files of the six DOFs of translation and rotation between registered time points. On the other hand, in the sequence of procedures for across-subject comparisons, the landmark-based approach is only a first approximation of the condyles, and

it is still necessary to compute correspondence to control for the across-subject variability.

Only rotations and translation parameters were considered in all registration approaches in this study, and no scaling was performed, because small condyles may be either indicative of the history of bone resorption or normal individual variability. As variability in size is normally present in populational/group studies, quantitative measures of differences between each individual condyle in the TMJ OA group compared with the control average were not reported in this study. Measures of individual variability have been recently applied to work in progress on imaging statistical modelling towards a diagnostic index of arthritic deformation that may still require larger control groups for adequate assessments of individual morphological variability.

As the aim of this study was to evaluate the reproducibility of the registration methods used, possible differences in the construction of the condylar surface models were eliminated with the use of the same surface model by both observers. Various segmentation methods have previously been validated, and although interobserver errors in segmentation present only small differences, these errors would be added to registration errors.[32,45,47,56] The artefacts generated from restorative dentistry, movement of the patient, partial volume averaging, incorrect selection of kVp/mA and threshold settings can affect the volume image and segmentation.[48,57–60] In the absence of artefacts, Luu et al[45] clearly described that when defining the true boundary of an object, at best, the line for this boundary will cross directly through the centre of a voxel. At worst, when attempting to select a boundary that truly goes between voxels, one is forced to select the centre of one of the surrounding voxels. In this study to reduce computational time, all CBCT images were reformatted to isotropic 0.5 mm voxels. The open-source image tools proposed in this study are robust and can be applied to smaller voxel sizes even at the micron level, at the expense of highly increased computational time. Considering quantitative approaches of condylar changes with no registration errors, the accuracy for the selection of a single voxel of 0.5 mm sides could be unavoidably off by the equivalent of half the diagonal of the voxel or 0.43. Given that a two point measurement requires the selection of two voxels, then, we would expect errors in accuracy to be as much as two voxel half–diagonal distances or around 0.86 mm.

Longitudinal assessments of changes in the bone morphology of the condyles require precise quantitative measurements between different time points. Registration of longitudinal images must be based on stable structures of reference.[61] An automatic voxel-based approach that uses thousands of voxels located in the region of interest was applied in this study to avoid observer-dependent landmark identification as shown in Figure 8. The voxel-based registration in this study extracted the mandibular condyles and neck as the region of interest, generating CBCT images that contained only the right or left condyle. The choice of the condyle and condylar neck as the region of reference for the voxel-based registration avoids including mandibular ramus areas that frequently present bone surface remodeling in patients with TMJ arthritis and/or following jaw surgery as shown in Figures 1 and 9. The interobserver error observed in the automated registration procedures in this study, although small, can be explained by slight differences in the observer-dependent

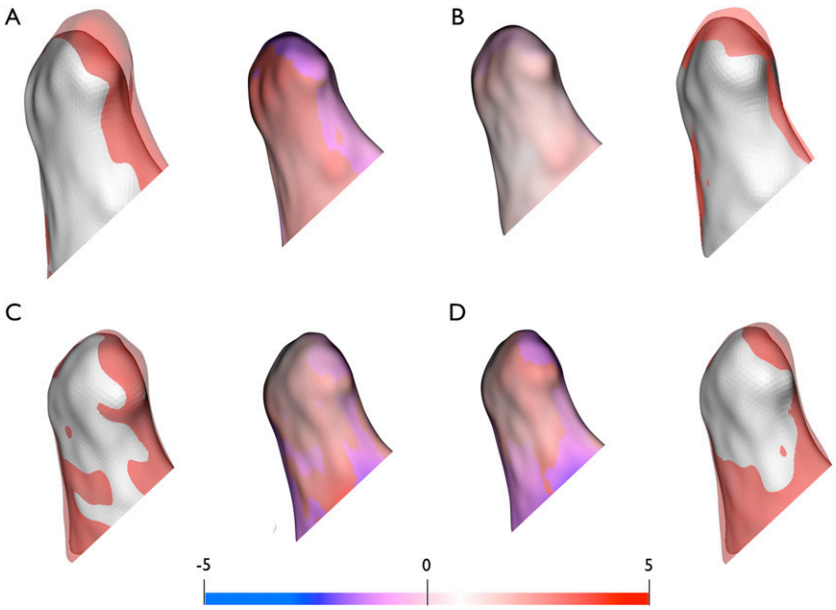

Figure 8 Comparison of interobserver variability in landmark-based *vs* voxel-based registration of a right condyle from pre-surgery to splint removal. Lateral views of overlaid condyles are shown. (a) Overlay resultant of landmark-based registration performed by Observer 1. (b) Overlay resultant of landmark-based registration performed by Observer 2. (c) Overlay resultant of voxel-based registration performed by Observer 1. (d) Overlay resultant of voxel-based registration performed by Observer 2. Colour visible in online version only

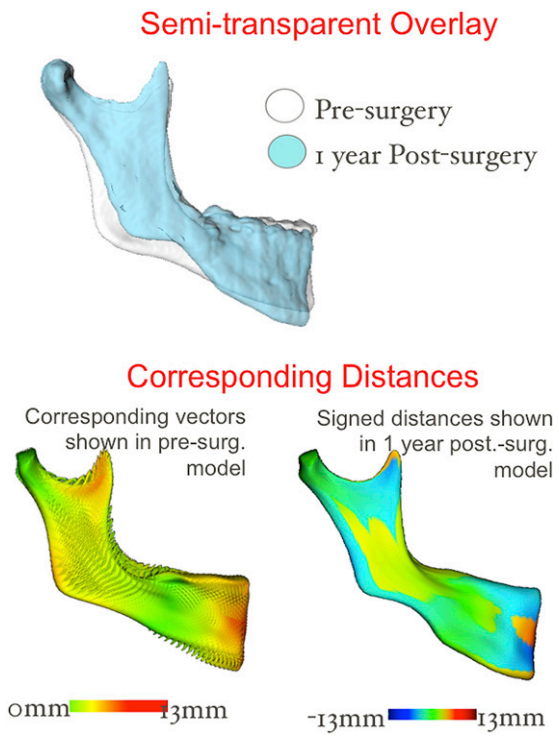

Figure 9 Marked ramus bone remodeling 1 year after two-jaw surgery. Surg, surgery. Colour visible in online version only

cropping of the anatomical region of interest. This study showed that mean interobserver differences were ≤0.6 mm in translation errors and 1.2° in rotation errors, with excellent reliability (ICC > 0.75).

The methods tested in this study have the potential to allow quantitative studies of arthritic condylar changes, shifting the focus on articular cartilage/disk to bone changes. TMJ differs from other joints because a layer of fibrocartilage, and not hyaline cartilage, covers it. The bone of the mandibular condyles is located just beneath the fibrocartilage, making it particularly vulnerable to inflammatory damage and a valuable model for studying arthritic bony changes. Although extensive assessments of OA in other joints have focused on loss or damage of hyaline cartilage,[62] the capacity of cartilage to repair and modify the surrounding extracellular matrix is limited in comparison to bone. The bone in TMJ condyle is the site of numerous dynamic morphological transformations, which are an integral part of the initiation/progression of OA, not merely secondary manifestations to cartilage degradation. Thus, a strong rationale exists for therapeutic approaches that target bone resorption and formation.

Conclusions

Condylar registration for across-subject and longitudinal assessments is reliable, and allows quantification of subtle bony differences in the 3D condylar morphology.

These registration methods have the potential to be used with other applications beyond the scope of this project. As part of the National Institutes of Health National Centers for Biomedical Computing program, the National Alliance for Medical Imaging Computing has implemented an open source platform that includes an end-user application (the 3D Slicer). This computational platform supports patient-specific decision making and assessment of the disease progression via registration of serial images.

References

1. Wang XD, Kou XX, Mao JJ, Gan YH, Zhou YH. Sustained inflammation induces degeneration of the temporomandibular joint. *J Dent Res* 2012; **91**: 499–505. doi: 10.1177/0022034512441946
2. Ogura N, Satoh K, Akutsu M, Tobe M, Kuyama K, Kuboyama N, et al. MCP-1 production in temporomandibular joint inflammation. *J Dent Res* 2010; **89**: 1117–1122. doi: 10.1177/0022034510376041
3. Kaneyama K, Segami N, Yoshimura H, Honjo M, Increased levels of soluble cytokine receptors in the synovial fluid of temporomandibular joint disorders in relation to joint effusion on magnetic resonance images. *J Oral Maxillofac Surg* 2010; **68**: 1088–1093. doi: 10.1016/j.joms.2009.10.027
4. Johnston JD, McLennan CE, Hunter DJ, Wilson DR. In vivo precision of a depth-specific topographic mapping technique in the CT analysis of osteoarthritic and normal proximal tibial subchondral bone density. *Skeletal Radiol* 2011; **40**: 1057–1064. doi: 10.1007/s00256-010-1001-6
5. Langs G, Peloschek P, Bischof H, Kainberger F. Automatic quantification of joint space narrowing and erosions in rheumatoid arthritis. *IEEE Trans Med Imaging* 2009; **28**: 151–164. doi: 10.1109/TMI.2008.2004401
6. Arnett GW, Gunson MJ. Risk factors in the initiation of condylar resorption. *Sem in Orthod* 2013; **19**: 81–88.
7. Gunson MJ, Arnett GW, Milam SB. Pathophysiology and pharmacologic control of osseous mandibular condylar resorption. *J Oral Maxillofac Surg* 2012; **70**: 1918–1934.
8. Dela Coleta KE, Wolford LM, Gonçalves JR, Pinto AS, Pinto LP, Cassano DS. Maxillo-mandibular counter-clockwise rotation and mandibular advancement with TMJ concepts total joint prostheses: part I–skeletal and dental stability. *Int J Oral Maxillofac Surg* 2009; **38**: 126–138.
9. Gonçalves JR, Cassano DS, Wolford LM, Santos-Pinto A, Márquez IM. Postsurgical stability of counterclockwise maxillomandibular advancement surgery: affect of articular disc repositioning. *J Oral Maxillofac Surg* 2008; **66**: 724–738.
10. Ahmad M, Hollender L, Anderson Q, Kartha K, Ohrbach RK, Truelove EL, et al. Research diagnostic criteria for temporomandibular disorders (RDC/TMD): development of image analysis criteria and examiner reliability for image analysis. *Oral Surg Oral Med Oral Pathol Oral Radiol Endod* 2009; **107**: 844–860.
11. Schiffman EL, Ohrbach R, Truelove EL, Tai F, Anderson GC, Pan W, et al. The Research Diagnostic Criteria for Temporomandibular Disorders. V: methods used to establish and validate revised Axis I diagnostic algorithms. *J Orofac Pain* 2010; **24**: 63–78.
12. Truelove E, Pan W, Look JO, Mancl LA, Ohrbach RK, Velly AM, et al. The Research Diagnostic Criteria for Temporomandibular Disorders. III: validity of Axis I diagnoses. *J Orofac Pain* 2010; **24**: 35–47.
13. Hussain AM, Packota G, Major PW, Flores-Mir C. Role of different imaging modalities in assessment of temporomandibular

joint erosions and osteophytes: a systematic review. *Dentomaxillofac Radiol* 2008; **37**: 63–71. doi: 10.1259/dmfr/16932758
14. Honey OB, Scarfe WC, Hilgers MJ, Klueber K, Silveira AM, Haskell BS, et al. Accuracy of cone-beam computed tomography imaging of the temporomandibular joint: comparisons with panoramic radiology and linear tomography. *Am J Orthod Dentofacial Orthop* 2007; **132**: 429–438. doi: 10.1016/j.ajodo.2005.10.032
15. Zain-Alabdeen EH, Alsadhan RI. A comparative study of accuracy of detection of surface osseous changes in the temporomandibular joint using multidetector CT and cone beam CT. *Dentomaxillofac Radiol* 2012; **41**: 185–191. doi: 10.1259/dmfr/24985981
16. Anker AH, D'Rozario RH, Li S. Computerized axial tomography in the diagnosis of internal derangements of the temporomandibular joint. *Aust Dent J* 1990; **35**: 253–257.
17. Hayashi T, Ito J, Koyama J, Hinoki A, Kobayashi F, Torikai Y, et al. Detectability of anterior displacement of the articular disk in the temporomandibular joint on helical computed tomography: the value of open mouth position. *Oral Surg Oral Med Oral Pathol Oral Radiol Endod* 1999; **88**: 106–111.
18. Cho BH, Jung YH. Osteoarthritic changes and condylar positioning of the temporomandibular joint in Korean children and adolescents. *Imaging Sci Dent* 2012; **42**: 169–174. doi: 10.5624/isd.2012.42.3.169
19. Liu MQ, Chen HM, Yap AU, Fu KY. Condylar remodeling accompanying splint therapy: a cone-beam computerized tomography study of patients with temporomandibular joint disk displacement. *Oral Surg Oral Med Oral Pathol Oral Radiol* 2012; **114**: 259–265. doi: 10.1016/j.oooo.2012.03.004
20. Zhang ZL, Cheng JG, Li G, Zhang JZ, Zhang ZY, Ma XC. Measurement accuracy of temporomandibular joint space in Promax 3-dimensional cone-beam computerized tomography images. *Oral Surg Oral Med Oral Pathol Oral Radiol* 2012; **114**: 112–117. doi: 10.1016/j.oooo.2011.11.020
21. Krisjane Z, Urtane I, Krumina G, Neimane L, Ragovska I. The prevalence of TMJ osteoarthritis in asymptomatic patients with dentofacial deformities: a cone-beam CT study. *Int J Oral Maxillofac Surg* 2012; **41**: 690–695. doi: 10.1016/j.ijom.2012.03.006
22. Alkhader M, Kuribayashi A, Ohbayashi N, Nakamura S, Kurabayashi T. Usefulness of cone beam computed tomography in temporomandibular joints with soft tissue pathology. *Dentomaxillofac Radiol* 2010; **39**: 343–348. doi: 10.1259/dmfr/76385066
23. Hajati AK, Alstergren P, Näsström K, Bratt J, Kopp S. Endogenous glutamate in association with inflammatory and hormonal factors modulates bone tissue resorption of the temporomandibular joint in patients with early rheumatoid arthritis. *J Oral Maxillofac Surg* 2009; **67**: 1895–1903. doi: 10.1016/j.joms.2009.04.056
24. Peterfy CG, Schneider E, Nevitt M. The osteoarthritis initiative: report on the design rationale for the magnetic resonance imaging protocol for the knee. *Osteoarthritis Cartilage* 2008; **16**: 1433–1441. doi: 10.1016/j.joca.2008.06.016
25. Helenius LM, Tervahartiala P, Helenius I, Al-Sukhun J, Kivisaari L, Suuronen R, et al. Clinical, radiographic and MRI findings of the temporomandibular joint in patients with different rheumatic diseases. *Int J Oral Maxillofac Surg* 2006; **35**: 983–989. doi: 10.1016/j.ijom.2006.08.001
26. Assaf AT, Kahl-Nieke B, Feddersen J, Habermann CR. Is high-resolution ultrasonography suitable for the detection of temporomandibular joint involvement in children with juvenile idiopathic arthritis? *Dentomaxillofac Radiol* 2013; **42**: 20110379.
27. Schellhas KP, Pollei SR, Wilkes CH. Pediatric internal derangements of the temporomandibular joint: effect on facial development. *Am J Orthod Dentofacial Orthop* 1993; **104**: 51–59.
28. Alexiou K, Stamatakis H, Tsiklakis K. Evaluation of the severity of temporomandibular joint osteoarthritic changes related to age using cone beam computed tomography. *Dentomaxillofac Radiol* 2009; **38**: 141–147. doi: 10.1259/dmfr/59263880
29. Slicer.org [homepage on the internet]. Boston: Surgical Planning Laboratory, Harvard Medical School [updated 22 July 2013; cited 22 July 2013]. Available from: http://download.slicer.org
30. Itksnap.org [homepage on the internet]. Philapelphia: Penn Image Computing and Science Laboratory, University of Pennsylvania [updated 17 April 2013; cited 22 July 2013]. Available from: http://www.itksnap.org/pmwiki/pmwiki.php?n=Main.Downloads
31. Yushkevich PA, Piven J, Hazlett HC, Smith RG, Ho S, Gee JC, et al. User-guided 3D active contour segmentation of anatomical structures: significantly improved efficiency and reliability. *Neuroimage* 2006; **31**: 1116–1128. doi: 10.1016/j.neuroimage.2006.01.015
32. Cevidanes LH, Hajati AK, Paniagua B, Lim PF, Walker DG, Palconet G, et al. Quantification of condylar resorption in temporomandibular joint osteoarthritis. *Oral Surg Oral Med Oral Pathol Oral Radiol Endod* 2010; **110**: 110–117. doi: 10.1016/j.tripleo.2010.01.008
33. Paniagua B, Cevidanes L, Walker D, Zhu H, Guo R, Styner M. Clinical application of SPHARM-PDM to quantify temporomandibular joint osteoarthritis. *Comput Med Imaging Graphics* 2011; **35**: 345–352. doi: 10.1016/j.compmedimag.2010.11.012
34. Imconvert [homepage on the internet]. North Carolina: Neuro Image Research and Analysis Laboratories, University of North Carolina.[updated 2004; cited 22 July 2013]. Available from: http://www.ia.unc.edu/dev/download/imconvert/index.htm
35. Canfieldsci.com [homepage on the internet]. Fairfield, NJ: Canfield Scientific, Inc [updated 02 July 2013; cited 22 July 2013]. Available from: http://www.canfieldsci.com
36. Styner M, Oguz I, Xu S, Brechbühler C, Pantazis D, Levitt JJ, et al. Framework for the Statistical Shape Analysis of Brain Structures using SPHARM-PDM. *Insight J* 2006; (1071): 242–250.
37. Neuroimaging Informatics Tools and Resources Clearinghouse (NITRC.org) Projects Spharm-PDM [homepage on the internet]. Chapel Hill, NC: Neuro Image Research and Analysis Laboratories, University of North Carolina [updated 21 July 2013; cited 22 July 2013]. Available from: http://www.nitrc.org/projects/spharm-pdm
38. Neuroimaging Informatics Tools and Resources Clearinghouse (NITRC.org) Projects Cmfreg [homepage on the internet]. Ann Arbor, MI: Dental and Craniofacial Bionetwork for Image Analysis, University of Michigan [updated 23 July 2013; cited 22 July 2013]. Available from: http://www.nitrc.org/projects/cmfreg
39. Neuroimaging Informatics Tools and Resources Clearinghouse (NITRC.org) Projects Shape Analysis Mancova [homepage on the internet]. Chapel Hill: Neuro Image Research and Analysis Laboratories, University of North Carolina [updated 27 June 2013; cited 22 July 2013]. Available from: http://www.nitrc.org/projects/shape_mancova
40. Paniagua B, Styner M, Macenko M, Pantazis D, Niethammer M. Local shape analysis using MANCOVA. *Insight Journal [serial on the internet]*. 2009 Sep [cited 22 July 2013; about 21 pp.]. Available from: http://www.insight-journal.org/browse/publication/694
41. Cevidanes LH, Styner MA, Proffit WR. Image analysis and superimposition of 3-dimensional cone-beam computed tomography models. *Am J Orthod Dentofacial Orthop* 2006; **129**: 611–618. doi: 10.1016/j.ajodo.2005.12.008
42. Geomagic.com [homepage on the internet]. Rock Hill, SC: 3D Systems Inc. [updated 18 July 2013; cited 22 July 2013]. Available from: http://www.geomagic.com/
43. Li P, Tang Y, Li J, Shen L, Tian W, Tang W. Establishment of sequential software processing for a biomechanical model of mandibular reconstruction with custom-made plate. *Comput Methods Programs Biomed* 2013; **111**: 642–649. doi: 10.1016/j.cmpb.2013.05.024
44. Anatomage.com [homepage on the Internet]. San Jose, CA: Anatomage [updated November 2012; cited 22 July 2013]. Available from: http://www.anatomage.com/product-Invivodental.html
45. Luu NS, Mandich MA, Flores-Mir C, El-Bialy T, Heo G, Carey JP, et al. The validity, reliability, and time requirement of study model analysis using cone-beam computed tomography-generated virtual study models. *Orthod Craniofac Res* Apr 2013. Epub ahead of print. doi: 10.1111/ocr.12024
46. Swennen GR, Mollemans W, De Clercq C, Abeloos J, Lamoral P, Lippens F, et al. A cone-beam computed tomography triple scan procedure to obtain a three-dimensional augmented virtual skull model appropriate for orthognathic surgery planning. *J Craniofac Surg* 2009; **20**: 297–307. doi: 10.1097/SCS.0b013e3181996803
47. Xi T, van Loon B, Fudalej P, Bergé S, Swennen G, Maal T. Validation of a novel semi-automated method for three-dimensional

surface rendering of condyles using cone beam computed tomography data. *Int J Oral Maxillofac Surg* 2013; **42**: 1023–1029. doi: 10.1016/j.ijom.2013.01.016
48. Kim M, Huh KH, Yi WJ, Heo MS, Lee SS, Choi SC. Evaluation of accuracy of 3D reconstruction images using multi-detector CT and cone-beam CT. *Imaging Sci Dent* 2012; **42**: 25–33. doi: 10.5624/isd.2012.42.1.25
49. Amira.com [homepage on the internet]. Burlington, MA: Visualization Sciences Group, Inc. [updated 11 July 2013; cited 22 July 2013]. Available from: http://www.amira.com/
50. VTK.org [homepage on the internet]. New York: Kitware, Inc. [updated 27 June 2013; cited 22 July 2013]. Available from: http://www.vtk.org/VTK/resources/software.html
51. Ibanez L, Schroeder W, Ng L, Cates J. The ITK software guide. New York: Kitware Inc; 2003.
52. ITK.org [homepage on the internet]. New York: Kitware, Inc. [updated 4 June 2013; cited 22 July 2013]. Available from: http://www.itk.org
53. CMake.org [homepage on the internet]. New York: Kitware, Inc. [updated 22 May 2013; cited 22 July 2013]. Available from: http://www.cmake.org/
54. Osirix-viewer.com [homepage on the internet]. Bernex, Switzerland: Pixmeo, Inc. [updated 01 Jul 2013; cited 22 Jul 2013]. Available from: http://www.osirix-viewer.com
55. Stratemann SA, Huang JC, Maki K, Hatcher DC, Miller AJ. Evaluating the mandible with cone-beam computed tomography. *Am J Orthod Dentofacial Orthop* 2010; **137**: S58–S70. doi: 10.1016/j.ajodo.2009.01.025
56. Fourie Z, Damstra J, Schepers RH, Gerrits PO, Ren Y. Segmentation process significantly influences the accuracy of 3D surface models derived from cone beam computed tomography. *Eur J Radiol* 2012; **81**: e524–e530. doi: 10.1016/j.ejrad.2011.06.001
57. Gultekin BA, Gultekin P, Leblebicioglu B, Basegmez C, Yalcin S. Clinical evaluation of marginal bone loss and stability in two types of submerged dental implants. *Int J Oral Maxillofac Implants* 2013; **28**: 815–823.
58. Barone A, Ricci M, Tonelli P, Santini S, Covani U. Tissue changes of extraction sockets in humans: a comparison of spontaneous healing vs. ridge preservation with secondary soft tissue healing. *Clin Oral Implants Res* Jul 2012. Epub ahead of print. doi: 10.1111/j.1600-0501.2012.02535.x
59. Kovacs M, Fejérdy P, Dobó NC. Metal artefact on head and neck cone-beam CT images. [Hungarian.]. *Fogorv Sz* 2008; **101**: 171–178.
60. Elstrøm UV, Muren LP, Petersen JB, Grau C. Evaluation of image quality for different kV cone-beam CT acquisition and reconstruction methods in the head and neck region. *Acta Oncol* 2011; **50**: 908–917. doi: 10.3109/0284186X.2011.590525
61. Johnston LE, Jr. Balancing the books on orthodontic treatment: an integrated analysis of change. *Br J Orthod* 1996; **23**: 93–102.
62. Loeser RF, Goldring SR, Scanzello CR, Goldring MB. Osteoarthritis: a disease of the joint as an organ. *Arthritis Rheum* 2012; **64**: 1697–1707. doi: 10.1002/art.34453